C. Brillante, M. Morandini, P. Mantegazza
Characterization of Beam Stiffness Matrix with Embedded Piezoelectric Devices via Generalized Eigenvectors
International Journal of Solids and Structures, Vol. 59, 2015, p. 37-45
doi:10.1016/j.ijsolstr.2015.01.003

Characterization of beam stiffness matrix with embedded piezoelectric devices via generalized eigenvectors

Claudio Brillante[a], Marco Morandini[a,*], Paolo Mantegazza[a]

[a] *Politecnico di Milano, Dipartimento di Scienze e Tecnologie Aerospaziali, via La Masa 34, 20156 Milano, ITALY*

Abstract

The formulation described in this paper leads to the electro-elastic characterization of the sectional properties of elastic anisotropic prismatic beam with embedded piezoelectric devices. The related matrix is derived by analyzing a set of two-dimensional electro-elastic problems defined on the beam section. These problems allow to compute both the so-called beam de Saint-Venant's solutions and the beam deformation field induced by an electric potential difference imposed between the piezoelectric conductive laminae. The results are compared to those obtained with three dimensional finite element models.

Keywords: Smart structures, active beam, beam section characterization, stiffness matrix, piezoelectric; de Saint-Venant.

1. Introduction

Piezoelectric devices are used for many different applications, either as actuators or sensors. Their relatively high operational bandwidth makes them suitable for applications where a reduction of structural vibration and noise radiation is sought (e.g. T C Manjunath, 2006; ur Rahman and Alam, 2012). A still valid review, albeit not very recent, about piezoelectric structures modeling can be found in (Benjeddou, 2000). Many applications involve piezoelectric devices embedded into slender beams. As an example, piezoelectric patches can be used to actively twist helicopter rotor blades. This solution should allow to reduce loads and vibrations in the fuselage, as shown by Shin and Censik (2007) and Ghiringhelli et al. (2008).

Three dimensional finite element models are often used to predict the response of beams with embedded piezelectric patches, e.g. in Rao et al. (2012). However, many works strives to avoid the complexity and cost of a full three dimensional model through simpler yet reliable models are being sought. The

*Corresponding author.

Email addresses: claudio.brillante@mail.polimi.it (Claudio Brillante), marco.morandini@polimi.it (Marco Morandini), paolo.mantegazza@polimi.it (Paolo Mantegazza)

simplest beam model is based on the Euler-Bernoulli approximation, as in Carpenter (1997), and R. Zemcik (2007). These works accounts only for the axial beam strain, and not for the change of dimension of the beam section. This allows to obtain an analytical expression for the cross-section properties. This kind of models can be improved by accounting for shear deformations, as proposed by Benjeddou et al. (1997) and Elshafei and Alraiess (2013). The former proposes a Timoshenko model for the core section and neglects the shear deformation for the external layers; the latter accounts for a parabolic distribution of the shear strain. It must be noted, though, that many of these specialized formulations must resort to constitutive equations specialized for an axial stress state. This fact, by itself, somewhat limits their applicability to the case of complex sections made of laminated composite materials. The use of mixed variational principles have been advocated by Maurini et al. (2004) to overcome the intrinsic limitations of the Euler-Bernoulli kinematic approximation.

In recent years countless papers on the beam sections structural properties characterization have been published; the interested reader can find a recent, partial overview in (Chakravarty, 2011). A general procedure for computing the stiffness matrix of a beam of arbitrarily complex geometry and made of composite materials was proposed by Giavotto et al. (1983). The procedure is based on a semi-analytical expansion of the unknown displacement field, with the stiffness matrix computed from the set of the so-called de Saint-Venant's solutions. To do so, the cross-section is discretized into finite elements, and the null eigenvalue solutions of a system of homogeneous second order differential equations along the beam axis are sought. Since then, many similar works have been published on the subject, some of them specializing the theory to the case of thin-walled beams. Among them, it is worth mentioning the works published by Hodges and his co-workers, who approach the problem aiming for an asymptotically correct solution. Their work is summarized in Hodges (2006). Following Giavotto et al. (1983) and Hodges (2006) extensions to the case of integrated piezoelectric devices were proposed by Ghiringhelli et al. (1997), Censik and Ortega-Morales (2001) and Roy et al. (2007).

A slightly different approach for the beam section characterization was proposed by Morandini et al. (2010). Starting fro Giavotto's work, Morandini et al. (2010) departs from it because they resort to the Hamiltonian structure of the solid beam differential equations, and do not add any (redundant) section rigid motion field to the section finite element displacement. This approach is strongly linked to Mielke's works on the de Saint-Venant's solutions (e.g. Mielke, 1991). A similar procedure, based on the works by Zong and co-workers, (e.g. Wanxie et al., 1996; Yao et al., 2009), was proposed by Bauchau and Han (in press).

This work extends Morandini et al. (2010) to electro-elastic beams. The related problem is first reformulated accounting for both the structural and the electric virtual work. It is then shown that, when piezoelectric effects have to be accounted for, the governing second order system of equations is no more homogeneous. Rather, it has the charge per unit span imposed on the electrodes as a forcing term. The generalized beam stiffness can thus be computed by accounting for both the homogeneous and the particular solutions of the system. Along

a similar line it is worth citing the work of Leung et al. (2008). They adopt the same formalism of Morandini et al. (2010), and recognize that piezoelectric materials can be accounted for by considering not only the solutions of the system but also the particular ones. However, they look for the analytical solution of a clamped beam, obtained accounting for both of the null eigenvalue solutions and of the decaying ones. They neither perform a finite element discretization of the beam section nor attempt to compute the generalized stiffness matrix of the beam.

The proposed approach should give, with the same mesh and finite element family, the same results that can be obtained by following Ghiringhelli et al. (1997), Censik and Ortega-Morales (2001) or Roy et al. (2007). The main difference between the proposed approach and the above mentioned works is conceptual. As explained above, all these works define the three dimensional displacement field by superposing a warping field onto the section motion. With the proposed approach, instead, the unknown displacement filed is defined without any redundancy. It is thus not necessary to further impose the indefinite equilibrium equations of the beam solving the three dimensional beam problem for a set of self-equilibrated internal forces, as in Ghiringhelli et al. (1997). As a consequence, it is no more required to assume that the average section motion of the three dimensional model coincides with that of the mono-dimensional beam model. Moreover, departing from Ghiringhelli et al. (1997), the electrodes equipotentiality constraint is naturally accounted for, without the need of modifying the equation set any more. Furthermore, each independent electrode requires now the solution of a single additional system of linear equations, while two were required in Ghiringhelli et al. (1997). Differently from Censik and Ortega-Morales (2001) and Roy et al. (2007), no asymptotic expansion is carried out. Thus, the result of the proposed procedure naturally leads to a beam stiffness matrix that does account for the shear deformation. In other words, it gives the actual stiffness matrix, computed from the so-called de Saint-Venant's solutions, of a given section, regardless of the beam length.

The paper is articulated as follows: the kinematical model and the equilibrium equations of the beam are first revised. The procedure to compute the stiffness matrix is then presented, and explained in three steps. Finally, some numerical examples are discussed.

2. Kinematical model and constitutive laws

Consider a geometrical model of a beam with the conventions of Fig. 1. Let $\boldsymbol{x}(\xi^1, \xi^2, \xi^3)$ be the position of a point in the reference configuration, where ξ^3 represents the coordinate along the straight axis of the beam and ξ^1 and ξ^2 are two local coordinates on the beam section. Assume the local coordinate ξ^3 to be perpendicular to the plane defined by ξ^1 and ξ^2 and, without loss of generality, coincident with the curvilinear abscissa s. The covariant base vector $\boldsymbol{g}_3 = \partial \boldsymbol{x}/\partial \xi^3$ is thus equal to the versor $\boldsymbol{n}$, normal to the ξ^1, ξ^2 plane; the covariant base vector coincides with and to the contravariant one, $\boldsymbol{g}_3 = \boldsymbol{g}^3 = \boldsymbol{n}$. Let $\boldsymbol{x}'(\xi^1, \xi^2, \xi^3)$ be the position of a point in the deformed configuration, so that

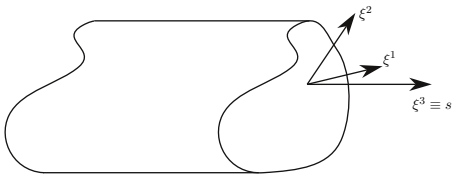

Figure 1: Straight beam geometry.

$\boldsymbol{u} = \boldsymbol{x}' - \boldsymbol{x}$ is the displacement of the point. The deformation gradient $\boldsymbol{F}$ is given by

$$\boldsymbol{F} = \boldsymbol{x}'_{/\otimes} = \boldsymbol{x}'_{/\otimes S} + \boldsymbol{x}'_{,3} \otimes \boldsymbol{g}^3 \tag{1}$$

where $\boldsymbol{g}^i$ are the three contravariant base vectors relative to the coordinates on the beam, $\boldsymbol{x}'_{/\otimes}$ stands for the gradient of vector $\boldsymbol{x}'$, $\boldsymbol{x}'_{/\otimes} = \boldsymbol{x}'_{,i} \otimes \boldsymbol{g}^i$ and $\boldsymbol{x}'_{/\otimes S} = \boldsymbol{x}'_{,1} \otimes \boldsymbol{g}^1 + \boldsymbol{x}'_{,2} \otimes \boldsymbol{g}^2$. The somewhat awkward notation $\boldsymbol{x}'_{/\otimes S}$ is introduced in order to decompose the deformation gradient $\boldsymbol{F}$ into a component along the direction of the beam axis and a term on the section plane. We are interested in the analysis of straight beams, with constant contravariant base vectors $\boldsymbol{g}^i$ along the span. The virtual variation of the deformation gradient is given by

$$\delta\boldsymbol{F} = \delta\boldsymbol{x}'_{/\otimes S} + \delta\boldsymbol{x}'_{,3} \otimes \boldsymbol{g}^3 \tag{2}$$

Assuming infinitesimal deformation and displacement field, the small strain tensor can be computed as

$$\boldsymbol{\epsilon} = \tfrac{1}{2}\left(\boldsymbol{F} + \boldsymbol{F}^T\right) - \boldsymbol{I} \tag{3}$$

Linear constitutive laws are considered for both the structural and the piezoelectric regions. The relation between the Cauchy stress tensor $\boldsymbol{S}$ and the small strain tensor $\boldsymbol{\epsilon}$ is given by

$$\boldsymbol{S} = \mathbb{E} : \boldsymbol{\epsilon}. \tag{4}$$

The piezoelectric constitutive law is

$$\left\{ \begin{array}{c} \boldsymbol{S} \\ \boldsymbol{D} \end{array} \right\} = \left[\begin{array}{cc} \mathbb{E} & -\mathcal{E}^{T231} \\ \mathcal{E} & \boldsymbol{\varepsilon} \end{array} \right] \left\{ \begin{array}{c} :\boldsymbol{\epsilon} \\ \cdot\boldsymbol{E} \end{array} \right\}, \tag{5}$$

where $\mathcal{E}$ and $\boldsymbol{\varepsilon}$ are the piezoelectric and the dielectric tensors, $\boldsymbol{D}$ is the dielectric displacement, the electric field $\boldsymbol{E}$ is equal to minus the gradient of the electric potential V,

$$\boldsymbol{E} = -V_{/\otimes} = -V_{/\otimes S} - V_{,3}\boldsymbol{g}^3, \tag{6}$$

and the operator $(\cdot)^{T231}$ applied to the third-order tensor $\mathcal{E} = \mathcal{E}_{ijk}\boldsymbol{g}^i \otimes \boldsymbol{g}^j \otimes \boldsymbol{g}^k$ transforms it into $\mathcal{E}^{T231} = \mathcal{E}_{ijk}\boldsymbol{g}^j \otimes \boldsymbol{g}^k \otimes \boldsymbol{g}^i$.

3. Virtual work principle

Consider the virtual work principle (VWP) for a beam of length L with end loads and electric charges q_C per unit surface imposed on the surface boundary ∂V_P

$$\begin{array}{c}\int_V \delta\boldsymbol{\epsilon} : \boldsymbol{S}\mathrm{d}V + \int_{V_p} \delta\boldsymbol{E}\cdot\boldsymbol{D}\mathrm{d}V_P = \int_A \delta\boldsymbol{x}'(L)\cdot\boldsymbol{f}(L)\mathrm{d}A + \int_A \delta\boldsymbol{x}'(0)\cdot\boldsymbol{f}(0)\mathrm{d}A \\ + \int_{A_P} \delta V(L)q(L)\mathrm{d}A_P + \int_{A_P} \delta V(0)q(0)\mathrm{d}A_P + \int_{\partial V_P} \delta V q_C \mathrm{d}\partial V_P\end{array} \tag{7}$$

where V_P is the volume of the piezoelectric regions, $\boldsymbol{E} = -V_{/\otimes}$ is understood, and q and q_C are the electric charges on the beam ends and the beam lateral surface, respectively. The electric charges are equal to the normal component of the electric displacement $\boldsymbol{D}$, $q = \boldsymbol{D}\cdot\boldsymbol{n}$. The integral $\int_{\partial V_P} \delta V q_C \mathrm{d}\partial V_P$ on the piezoelectric surface boundary ∂V_P is understood to be carried out only on the surface where the potential V is left free, i.e. where the surface charge can be imposed; wherever the potentials were imposed the electric charge would be unknown.

Following a well-consolidated procedure (e.g. Giavotto et al. 1983; Morandini et al. 2010) Eq. (7) can be transformed by integrating by part all the terms that have, as virtual variation, the derivative with respect to ξ^3 of either the deformed position vector $\boldsymbol{x}'$ or the electric potential V. This allows to transform Eq. (7) into a set of two differential equations in the ξ^3 direction. In doing so the volume integral involving the contravariant base vector $\boldsymbol{g}^3$ can be evaluated as $\int_V (\cdot)\boldsymbol{g}^3\mathrm{d}V = \int_L \int_A (\cdot)\boldsymbol{n}\mathrm{d}A\mathrm{d}\xi^3$, where A is the surface spanned by $\{\xi^1, \xi^2\}|_{\xi^3=\mathrm{const}}$. Integration by part leads to

$$\begin{array}{c}-\int_{V_P} \delta V_{/\otimes S}\cdot\boldsymbol{D}\mathrm{d}V_P + \int_{V_P} \delta V \boldsymbol{n}\cdot\boldsymbol{D}_{,3}\mathrm{d}A_P\mathrm{d}\xi^3 - \left[\int_{A_P} \delta V\left(\boldsymbol{n}\cdot\boldsymbol{D} - q\right)\mathrm{d}A_P\right]_L \\ + \left[\int_{A_P} \delta V\left(\boldsymbol{n}\cdot\boldsymbol{D} - q\right)\mathrm{d}A_P\right]_0 = \int_{\partial V_P} \delta V q_C \mathrm{d}\partial V_P,\end{array} \tag{8}$$

$$\begin{array}{rcl}-\int_V \delta\boldsymbol{x}'\otimes\boldsymbol{n} : \boldsymbol{S}_{,3}\mathrm{d}A\mathrm{d}\xi^3 + \int_V \delta\boldsymbol{x}'_{/\otimes S} : \boldsymbol{S}\mathrm{d}A\mathrm{d}\xi^3 & & \\ + \left[\int_A \delta\boldsymbol{x}'\cdot(\boldsymbol{S}\cdot\boldsymbol{n} - \boldsymbol{f})\right]_L - \left[\int_A \delta\boldsymbol{x}'\cdot(\boldsymbol{S}\cdot\boldsymbol{n} - \boldsymbol{f})\right]_0 & = & 0.\end{array} \tag{9}$$

Equation (9) is derived taking into account the symmetry of the stress tensor, so that $\delta\boldsymbol{\epsilon} : \boldsymbol{S} = \delta\boldsymbol{F} : \boldsymbol{S}$. Using the constitutive law Eq. (5) and the definitions of the small strain tensor $\boldsymbol{\epsilon}$ and electric field vector $\boldsymbol{E}$, Eqs. (3, 6), into Eqs. (8, 9) introduces the second derivative of the deformed position and electric potential, $\boldsymbol{x}'_{,33}$ and $V_{,33}$, and brings the equations to their final form. The terms at the boundary are nothing but the definition of the natural boundary conditions.

Equations (8, 9) can be reduced to a set of second order ordinary differential equations with a finite number of unknowns by using a finite element approximation. To do so, the unknown displacement $\boldsymbol{u} = \boldsymbol{x}' - \boldsymbol{x}$ and electric potential V are interpolated over the cross sections by means of suitable interpolating functions N_{pi} and N_i, and the nodal values of the electric potential V_i and displacement $\boldsymbol{u}_i$ are assumed to be functions of the ξ^3 coordinate:

$$\begin{array}{c}V = \sum_i N_{pi}(\xi^1, \xi^2)V_i(\xi^3), \\ \boldsymbol{u} = \sum_i N_i(\xi^1, \xi^2)\boldsymbol{u}_i(\xi^3).\end{array} \tag{10}$$

The final result is the following set of second-order differential equations in the nodal unknowns:

$$\begin{bmatrix} \boldsymbol{M}_{uu} & \boldsymbol{M}_{uV} \\ \boldsymbol{M}_{uV}^T & -\boldsymbol{M}_{VV} \end{bmatrix} \begin{Bmatrix} \boldsymbol{u}_{,33} \\ \boldsymbol{V}_{,33} \end{Bmatrix} + \begin{bmatrix} \left(\boldsymbol{C}_{uu}^T - \boldsymbol{C}_{uu}\right) & \left(\boldsymbol{C}_{Vu}^T - \boldsymbol{C}_{uV}\right) \\ \left(\boldsymbol{C}_{uV}^T - \boldsymbol{C}_{Vu}\right) & \left(\boldsymbol{C}_{VV} - \boldsymbol{C}_{VV}^T\right) \end{bmatrix} \begin{Bmatrix} \boldsymbol{u}_{,3} \\ \boldsymbol{V}_{,3} \end{Bmatrix} + \begin{bmatrix} -\boldsymbol{E}_{uu} & -\boldsymbol{E}_{uV} \\ -\boldsymbol{E}_{uV}^T & \boldsymbol{E}_{VV} \end{bmatrix} \begin{Bmatrix} \boldsymbol{u} \\ \boldsymbol{V} \end{Bmatrix} = \begin{Bmatrix} \boldsymbol{0} \\ \boldsymbol{Q}_C \end{Bmatrix}, \tag{11}$$

or, with a more compact notation,

$$\boldsymbol{M} \begin{Bmatrix} \boldsymbol{u}_{,33} \\ \boldsymbol{V}_{,33} \end{Bmatrix} + \boldsymbol{H} \begin{Bmatrix} \boldsymbol{u}_{,3} \\ \boldsymbol{V}_{,3} \end{Bmatrix} + \boldsymbol{E} \begin{Bmatrix} \boldsymbol{u} \\ \boldsymbol{V} \end{Bmatrix} = \begin{Bmatrix} \boldsymbol{0} \\ \boldsymbol{Q}_C \end{Bmatrix}. \tag{12}$$

Explicit expressions for the matrices of Eq. 11 are reported in the Appendix. Note that the matrix $\boldsymbol{E}_{uu}$ is four times singular because of three rigid translations and of the rigid rotation around the beam section ξ^3 axis. These rigid body motions must be constrained. The matrix $\boldsymbol{E}_{VV}$ is singular as well, because the electric potential is defined up to an independent constant for each independent electric region. Thus, it is singular as many times as the number of the independent piezoelectric regions. Conductive surfaces, i.e. equipotential surfaces, are not modeled explicitly, but they are represented by the nodes on the boundaries of each piezoelectric device. The same equation number is given to the nodes which represent the same electrode, so to satisfy the equipotentiality constraint along the section plane[1]. Therefore, each electrode has a unique electric potential. Constraining the potential value of one electrode for each independent piezoelectric region brings matrix $\boldsymbol{E}_{VV}$ to full rank.

4. Beam section characterization

Consider the internal work of the piezoelectric beam

$$\delta L_i = \int_V \delta\boldsymbol{\epsilon} : \boldsymbol{S} dV + \int_{V_p} \delta\boldsymbol{E} \cdot \boldsymbol{D} dV_P \tag{13}$$

By following the same steps of the previous sections but without integrating by part, the internal work is equal to

$$\delta L_i = \int_L \begin{Bmatrix} \delta\boldsymbol{u}_{,3} \\ \delta\boldsymbol{V}_{,3} \\ \delta\boldsymbol{u} \\ \delta\boldsymbol{V} \end{Bmatrix}^T \begin{bmatrix} \boldsymbol{M}_{uu} & \boldsymbol{M}_{uV} & \boldsymbol{C}_{uu}^T & \boldsymbol{C}_{Vu}^T \\ -\boldsymbol{M}_{uV}^T & \boldsymbol{M}_{VV} & -\boldsymbol{C}_{uV}^T & \boldsymbol{C}_{VV}^T \\ \boldsymbol{C}_{uu} & \boldsymbol{C}_{uV} & \boldsymbol{E}_{uu} & \boldsymbol{E}_{uV} \\ -\boldsymbol{C}_{Vu} & \boldsymbol{C}_{VV} & -\boldsymbol{E}_{uV}^T & \boldsymbol{E}_{VV} \end{bmatrix} \begin{Bmatrix} \boldsymbol{u}_{,3} \\ \boldsymbol{V}_{,3} \\ \boldsymbol{u} \\ \boldsymbol{V} \end{Bmatrix} \mathrm{d}\xi^3 \ , \tag{14}$$

or, with a shorter notation

$$\delta L_i = \int_L \delta\boldsymbol{q}^T \boldsymbol{K}_{FEM} \boldsymbol{q} \mathrm{d}\xi^3, \tag{15}$$

[1] Equipotentiality along the beam axis will be imposed in the stiffness matrix computation.

where $\boldsymbol{q} = \left\{ \begin{array}{cccc} \boldsymbol{u}_{,3}^T & \boldsymbol{V}_{,3}^T & \boldsymbol{u}^T & \boldsymbol{V}^T \end{array} \right\}^T$ is the $(N \times 1)$ vector of state variables.

As in (Morandini et al., 2010), the stiffness matrix of the beam is recovered by projecting the three dimensional problem into a suitable vector space. Therefore the six generalized deformations $\boldsymbol{\psi}$ of the beam energetically conjugated to the internal forces and to the electric potentials applied on the n_C independent electrodes $\boldsymbol{V}_C$ become the new generalized coordinates. We then assume that the state variable $\boldsymbol{q}$ can be approximated as

$$\boldsymbol{q} \approx \left[\boldsymbol{Q}_{st} \, \boldsymbol{Q}_p \right] \left\{ \begin{array}{c} \boldsymbol{\psi} \\ \boldsymbol{V}_C \end{array} \right\}, \tag{16}$$

where matrices $\boldsymbol{Q}_{st}$ and $\boldsymbol{Q}_p$ are $(N \times 6)$ and $(N \times n_c)$, respectively. The matrix $\boldsymbol{Q}_{st}$ represents the beam section behavior for a null electrode electric potential, i.e. for null forcing terms in Eq. (11). The matrix $\boldsymbol{Q}_p$, instead, describes the beam behavior whenever an electric potential is applied, i.e. describes a particular solution of Eq. (11). Substituting (16) into Eq. (15) leads to

$$\delta L_i = \int_L \delta \left\{ \begin{array}{c} \boldsymbol{\psi}^T \\ \boldsymbol{V}_C^T \end{array} \right\} \left[\boldsymbol{Q}_{st} \, \boldsymbol{Q}_p \right]^T \boldsymbol{K}_{FEM} \left[\boldsymbol{Q}_{st} \, \boldsymbol{Q}_p \right] \left\{ \begin{array}{c} \boldsymbol{\psi} \\ \boldsymbol{V}_C \end{array} \right\} \mathrm{d}\xi^3. \tag{17}$$

The virtual work per unit length of the beam is the work of the generalized internal forces $\boldsymbol{\vartheta}$ and of the imposed electrodes charges $\boldsymbol{Q}_c$ for the virtual variations of the beam generalized deformations $\delta\boldsymbol{\psi}$ and of the electrodes potential $\delta\boldsymbol{V}_c$, respectively. It must be equal to the virtual work of the corresponding three dimensional solid, i.e. to the integrand of Eq. (17). For a beam with linear constitutive laws the internal forces $\boldsymbol{\vartheta}$ and electric charges $\boldsymbol{Q}_c$ can be computed as

$$\left\{ \begin{array}{c} \boldsymbol{\vartheta} \\ \boldsymbol{Q}_c \end{array} \right\} = \left[\begin{array}{cc} \boldsymbol{K}_{\psi\psi} & \boldsymbol{K}_{\psi V} \\ -\boldsymbol{K}_{\psi V}^T & \boldsymbol{K}_{VV} \end{array} \right] \left\{ \begin{array}{c} \boldsymbol{\psi} \\ \boldsymbol{V}_C \end{array} \right\},$$

where the section stiffness matrix $\boldsymbol{K}_{\psi\psi}$, the actuation/sensor matrix $\boldsymbol{K}_{\psi V}$ and the capacitance matrix $\boldsymbol{K}_{VV}$ define the overall generalized stiffness of the beam section and have dimension of (6×6), $(6 \times n_C)$ and $(n_C \times n_C)$, respectively. Theerefore, the following relation must hold

$$\left\{ \begin{array}{c} \delta\boldsymbol{\psi} \\ \delta\boldsymbol{V}_C \end{array} \right\}^T \left[\begin{array}{cc} \boldsymbol{K}_{\psi\psi} & \boldsymbol{K}_{\psi V} \\ -\boldsymbol{K}_{\psi V}^T & \boldsymbol{K}_{VV} \end{array} \right] \left\{ \begin{array}{c} \boldsymbol{\psi} \\ \boldsymbol{V}_C \end{array} \right\} = \left\{ \begin{array}{c} \delta\boldsymbol{\psi} \\ \delta\boldsymbol{V}_C \end{array} \right\}^T \left[\boldsymbol{Q}_{st} \, \boldsymbol{Q}_p \right]^T \boldsymbol{K}_{FEM} \left[\boldsymbol{Q}_{st} \, \boldsymbol{Q}_p \right] \left\{ \begin{array}{c} \boldsymbol{\psi} \\ \boldsymbol{V}_C \end{array} \right\} \tag{18}$$

for every possible $\delta\boldsymbol{\psi}$, $\delta\boldsymbol{V}_C$, $\boldsymbol{\psi}$ and $\boldsymbol{V}_C$, so that the beam section stiffness matrix can be computed as

$$\left[\begin{array}{cc} \boldsymbol{K}_{\psi\psi} & \boldsymbol{K}_{\psi V} \\ -\boldsymbol{K}_{\psi V}^T & \boldsymbol{K}_{VV} \end{array} \right] = \left[\boldsymbol{Q}_{st} \, \boldsymbol{Q}_p \right]^T \boldsymbol{K}_{FEM} \left[\boldsymbol{Q}_{st} \, \boldsymbol{Q}_p \right].$$

The problem is to compute meaningful matrices $\boldsymbol{Q}_{st}$ and $\boldsymbol{Q}_p$, such that Eq. (16) do well approximate the overall beam behavior. The procedure, already explained in Morandini et al. (2010) for the matrix $\boldsymbol{Q}_{st}$, is discussed in the following paragraphs. The two matrices $\boldsymbol{Q}_{st}$ and $\boldsymbol{Q}_p$ can be computed independently and the computation of the stiffness matrix requires three steps:

1. a linear combination $\tilde{\boldsymbol{Q}}_{st}$ of the columns of $\boldsymbol{Q}_{st}$ is determined in Section 4.1 by exploiting the homogeneous problem of equations (11) with the electrodes of each independent piezoelectric region short–circuited;
2. the matrix $\boldsymbol{Q}_p$ is determined in Section 4.2 by computing the particular solution of the problem (11); this can be accomplished either by imposing the electric charge per unit length on the electrodes, and solving for the unknown independent electrodes potential, or by directly imposing the potentials and computing the unknown charges.
3. the matrix $\boldsymbol{Q}_{st}$ is computed from $\tilde{\boldsymbol{Q}}_{st}$ in Section 4.3 by imposing that the beam generalized deformations must be, by definition, energetically conjugated to the internal forces computed for the three dimensional beam model.

The procedure is detailed in Sections 4.1–4.3 below.

4.1. Homogeneous solution

Equations (12) can be reduced to a system of first order differential equations

$$\begin{bmatrix} \boldsymbol{M} & \boldsymbol{0} \\ \boldsymbol{0} & \boldsymbol{I} \end{bmatrix} \boldsymbol{q}_{,3} = \begin{bmatrix} -\boldsymbol{H} & -\boldsymbol{E} \\ \boldsymbol{I} & \boldsymbol{0} \end{bmatrix} \boldsymbol{q} + \begin{Bmatrix} \boldsymbol{Q}_C \\ \boldsymbol{0} \end{Bmatrix} \tag{19}$$

or, with a shorter descriptor form notation

$$\boldsymbol{D}\boldsymbol{q}_{,3} = \boldsymbol{A}\boldsymbol{q} + \boldsymbol{B}\boldsymbol{Q}_C. \tag{20}$$

The first term of the vector base $\tilde{\boldsymbol{Q}}_{st}$ can be determined through the solution of the homogeneous problem of Eq. (20) with short–circuited electrodes. The piezoelectric electrodes equipotentiality along the beam axis implies that not only the electrode potentials are null, but also their derivatives. The homogeneous short–circuited problem

$$\tilde{\boldsymbol{q}}_{,3} \quad = \quad \tilde{\boldsymbol{A}}\tilde{\boldsymbol{q}} \tag{21}$$

has 12 null eigenvalues, as shown in (Morandini et al., 2010). The solutions corresponding to the null eigenvalues are organized in four polynomial Jordan chains; each chain originates from one of the four rigid body motions of the section, and represent the central solution of the beam. Two polynomial chains grows up to a third order polynomial, while the other two grow up to a linear polynomial. All the remaining solutions of the homogeneous short–circuited problem are exponentially decaying, and are called extremity solutions. Since we are neglecting end effects we are interested in the polynomial solutions only. The sought fourth polynomial solutions assume the following form

$$\tilde{\boldsymbol{q}} = \begin{bmatrix} \boldsymbol{x}_1 & \boldsymbol{x}_2 & \boldsymbol{x}_3 & \boldsymbol{x}_4 \end{bmatrix} \begin{bmatrix} 1 & \xi^3 & \frac{(\xi^3)^2}{2} & \frac{(\xi^3)^3}{6} \\ 0 & 1 & \xi^3 & \frac{(\xi^3)^2}{2} \\ 0 & 0 & 1 & \xi^3 \\ 0 & 0 & 0 & 1 \end{bmatrix} \boldsymbol{k}, \tag{22}$$

where vector $\boldsymbol{k}$ defines the amplitude of each polynomial. The generalized eigenvectors $\boldsymbol{x}_i$, $i = \{1, 2, 3, 4\}$ of the homogeneous problem can be computed by resolving a set of system of linear equations:

$$\begin{array}{rcl} \boldsymbol{E}\boldsymbol{d}_0 & = & 0 \\ \boldsymbol{E}\boldsymbol{d}_1 & = & -\boldsymbol{H}\boldsymbol{d}_0 \\ \boldsymbol{E}\boldsymbol{d}_i & = & -\boldsymbol{H}\boldsymbol{d}_{i-1} - \boldsymbol{M}\boldsymbol{d}_{i-2},\ i \geq 2 \end{array} \tag{23}$$

Note that a similar approach was suggested also by Aldraihem and Khdeir (2000). The initial eigenvectors $\boldsymbol{d}_0$ are known beforehand: they represent the four rigid motions stemming from the null space of $\boldsymbol{E}$. In fact, matrix $\boldsymbol{E}$ is four times singular and has to be constrained while resolving the Jordan chains. The resulting generalized eigenvectors are computed as follows

$$\boldsymbol{x}_1 = \begin{bmatrix} \boldsymbol{0} \\ \boldsymbol{d}_0 \end{bmatrix} \quad \dots \quad \boldsymbol{x}_i = \begin{bmatrix} \boldsymbol{d}_{i-1} \\ \boldsymbol{d}_i \end{bmatrix} \tag{24}$$

Once the 12 generalized eigenvectors are computed, the vector base $\boldsymbol{Q}_{st}$ is constructed by using only the 6 eigenvectors which contribute to the deformation of the beam. These vectors are respectively the last two vectors associated to the bending and the last vector related to the axial and to the torsional rigid motions:

$$\tilde{\boldsymbol{Q}}_{st} = \begin{bmatrix} \boldsymbol{x}_{3bend1} & \boldsymbol{x}_{4bend1} & \boldsymbol{x}_{3bend2} & \boldsymbol{x}_{4bend2} & \boldsymbol{x}_{2axial} & \boldsymbol{x}_{2torsional} \end{bmatrix}. \tag{25}$$

4.2. Particular solution

In order to compute the vector base $\boldsymbol{Q}_p$ we exploit the particular solution of Eq. (12). This allows to compute the solution when an electric potential is applied to the electrodes. Since the applied potential $\boldsymbol{V}_c$ is constant, the particular solution is constant as well. Considering Eq. (12), the particular solution is given by

$$\boldsymbol{E} \left\{ \begin{array}{c} \boldsymbol{u} \\ \boldsymbol{V} \end{array} \right\}_{pt} = \left\{ \begin{array}{c} \boldsymbol{0} \\ \boldsymbol{Q}_C \end{array} \right\}. \tag{26}$$

As stated before, the matrix $\boldsymbol{Q}_p$ can be computed either by imposing the electric charge per unit length on the electrodes, or by directly imposing the electric potentials. If the first approach is used, unit and opposite charges $\boldsymbol{Q}_C$ are applied at the master and slave electrode for each piezoelectric region and the solution $\left\{ \begin{array}{c} \boldsymbol{u} \\ \boldsymbol{V} \end{array} \right\}_{pt}$ is then computed. Since we are interested in the behavior of the beam under unit applied electric potential at the electrodes $\boldsymbol{V}_C$, and not to unit charge, the matrix built with the different solutions as columns must be multiplied on the right by the inverse matrix of the electrodes electric potentials. If the second approach is used instead, i.e. if the solution is directly computed by applying unit electric potential difference on each piezoelectric region, no post-processing is required.

Since the particular solution is constant, its derivative is zero and the sought vector base $\boldsymbol{Q}_p$ is

$$\boldsymbol{Q}_p \quad = \quad \left[\begin{array}{c} \boldsymbol{0} \\ \left\{ \begin{array}{c} \boldsymbol{u} \\ \boldsymbol{V} \end{array} \right\}_{pt} \end{array} \right] \tag{27}$$

4.3. Computation of the generalized beam stiffness matrix

Having computed the generalized eigenvectors $\tilde{\boldsymbol{Q}}_{st}$ and the solution $\boldsymbol{Q}_p$ for applied unit potential on the electrodes $\boldsymbol{V}_C$ the state variable vector $\boldsymbol{q}$ can be approximated as

$$\boldsymbol{q} = \left[\tilde{\boldsymbol{Q}}_{st} \, \boldsymbol{Q}_p \right] \left\{ \begin{array}{c} \boldsymbol{k}_d \\ \boldsymbol{V}_C \end{array} \right\} \tag{28}$$

where vector $\boldsymbol{k}_d$ defines the amplitude of the 6 eigenvectors. However, vector $\boldsymbol{k}_d$ is not, in general, energetically conjugated to the internal forces of the beam. A further step is thus needed in order to compute the correct stiffness matrix. Following the same approach of Morandini et al. (2010), a coordinate transformation $\boldsymbol{G}$ is sought for the short–circuited solutions so that

$$\boldsymbol{k}_d = \boldsymbol{G}\boldsymbol{\psi}. \tag{29}$$

This is equivalent to trasnform the state variable vector $\boldsymbol{q}$ through a linear combination of the columns of matrix $\boldsymbol{Q}_{st} = \tilde{\boldsymbol{Q}}_{st}\boldsymbol{G}$. Consider the internal work per unit length of the beam (15) projected onto $\boldsymbol{k}_d$:

$$\delta\tilde{L}_i = \delta\boldsymbol{\psi}^T \boldsymbol{G}^T \tilde{\boldsymbol{Q}}_{st}^T \boldsymbol{K}_{FEM} \tilde{\boldsymbol{Q}}_{st} \boldsymbol{G}\boldsymbol{\psi} = \delta\boldsymbol{\psi}^T \boldsymbol{G}^T \widetilde{\boldsymbol{K}} \boldsymbol{G}\boldsymbol{\psi}. \tag{30}$$

The transformation matrix $\boldsymbol{G}$ is obtained by imposing that the internal work of Eq. (30) must be equal to the external work. Since the piezoelectric regions are kept short–circuited the external work is equal to the product of the virtual generalized deformations and the internal forces of the beam,

$$\delta\tilde{L}_{istruct} = \delta\boldsymbol{\psi}^T \boldsymbol{\vartheta}, \tag{31}$$

where the internal forces are defined as

$$\boldsymbol{\vartheta} = \int_A \left[\begin{array}{c} \boldsymbol{I} \\ \boldsymbol{x}_\times \end{array} \right] \boldsymbol{S} \cdot \boldsymbol{n} dA. \tag{32}$$

Consider the constitutive law $\boldsymbol{S} = \mathbb{E}\boldsymbol{\epsilon} - \boldsymbol{e}^T\boldsymbol{E}$ and Eqs. (1) and (6). The structural external work can be computed as

$$\delta\tilde{L}_{istruct} = \delta\boldsymbol{\psi}^T \left[\begin{array}{cccc} \boldsymbol{L}^T & \boldsymbol{Y}^T & \boldsymbol{R}^T & \boldsymbol{Z}^T \end{array} \right] \tilde{\boldsymbol{Q}}_{st} \boldsymbol{k}_d = \delta\boldsymbol{\psi}^T \left[\begin{array}{cccc} \boldsymbol{L}^T & \boldsymbol{Y}^T & \boldsymbol{R}^T & \boldsymbol{Z}^T \end{array} \right] \tilde{\boldsymbol{Q}}_{st} \boldsymbol{G}\boldsymbol{\psi}, \tag{33}$$

where the matrices $\boldsymbol{L}$, $\boldsymbol{Y}$, $\boldsymbol{R}$ and $\boldsymbol{Z}$ are computed from Eq. (32) with the finite element discretization of Eq. (10). Equating Eqs. (30) and (33) leads to

$$\delta\boldsymbol{\psi}^T \boldsymbol{G}^T \widetilde{\boldsymbol{K}} \boldsymbol{G}\boldsymbol{\psi} = \delta\boldsymbol{\psi}^T \left[\begin{array}{cccc} \boldsymbol{L}^T & \boldsymbol{Y}^T & \boldsymbol{R}^T & \boldsymbol{Z}^T \end{array} \right] \tilde{\boldsymbol{Q}}_{st} \boldsymbol{G}\boldsymbol{\psi}. \tag{34}$$

Piezoelectric (PZ21)	
$E_{11} = E_{22}$, Gpa	5.9017E+1
E_{33}, GPa	4.0906E+1
ν_{12}	0.3413
$\nu_{13} = \nu_{23}$	0.3856
$G_{12} = G_{23} = G_{13}$, GPa	2.2E+1
$\mathcal{E}_{311}$, C/m^2	-5.3979
$\mathcal{E}_{322}$, C/m^2	-5.3979
$\mathcal{E}_{333}$, C/m^2	2.2836E+1
$\epsilon_{11} = \epsilon_{22}$, F/m	3.1892E-8
ϵ_{33}, F/m	1.3846E-8

Table 1: Piezoelectric material properties.

Note that only the structural deformations have to be transformed. Equation (34) must be verified for every possible deformation $\boldsymbol{G\psi}$, so it is equivalent to a system of linear equations

$$\widetilde{\boldsymbol{K}}^T \boldsymbol{G} = \tilde{\boldsymbol{Q}}_{st}^T \left[\begin{array}{cccc} \boldsymbol{L}^T & \boldsymbol{Y}^T & \boldsymbol{R}^T & \boldsymbol{Z}^T \end{array} \right]^T . \tag{35}$$

Then the sought coordinate transformation $\boldsymbol{G}$ can be found by solving Eq. (35). The generalized stiffness matrix $\boldsymbol{K}$ of the beam section can finally be computed as

$$\boldsymbol{K} = \left[\begin{array}{cc} \boldsymbol{G} & \boldsymbol{0} \\ \boldsymbol{0} & \boldsymbol{I} \end{array} \right]^T \left[\tilde{\boldsymbol{Q}}_{st} \boldsymbol{Q}_p \right]^T \boldsymbol{K}_{FEM} \left[\tilde{\boldsymbol{Q}}_{st} \boldsymbol{Q}_p \right] \left[\begin{array}{cc} \boldsymbol{G} & \boldsymbol{0} \\ \boldsymbol{0} & \boldsymbol{I} \end{array} \right] . \tag{36}$$

5. Examples

The first two examples deal with beams made of homogeneous material and thin piezoelectric patches. The host structure material is an isotropic epoxy resin with elastic modulus $E = 3.5$ GPa and Poisson coefficient $\nu = 0.34$. An orthotropic piezoceramic material is used for the piezoelectric patches. Table 1 reports the piezoelectric material properties computed in a local coordinate system, with the polarization applied in the direction of the local z axis. The stiffness matrix computed with the proposed method is compared with results obtained using the software Abaqus and, when available, with literature results obtained with the software ANBA (Ghiringhelli et al., 1997) and VABS (Roy et al., 2007).

5.1. Example 1 : Beam with two piezoelectric patches

In this example a rectangular beam section with two piezoelectric actuators is considered. Two piezoelectric patches are attached on the upper and lower faces of the beam, as shown in Fig. 2. The beam core is 0.1x0.05 m and the piezoelectric patches are 0.002 m thick. The beam section is discretized with a 6x6 mesh, the piezoelectric patches with one element through the thickness.

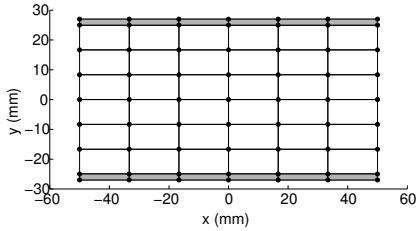

Figure 2: Rectangular section.

$\boldsymbol{K}_{\psi\psi}$		$\boldsymbol{K}_{\psi V}$		$\boldsymbol{K}_{VV}$	
EA, N	4.1107E+07	T_{zV1}, C/m	1.627	C_{ii}, F/m	1.2688E-6
$(GA)_x$, N	1.3074E+07	T_{zV2}, C/m	1.627	C_{ij}, F/m	-2.1555E-8
$(GA)_y$, N	6.8735E+06	M_{xV1}, C	-4.254E-2		
GJ, Nm^2	1.2050E+4	M_{xV2}, C	4.254E-2		
$(EJ)_x$, Nm^2	1.9673E+4				
$(EJ)_y$, Nm^2	3.4482E+4				

Table 2: Rectangular section beam properties.

The electrodes are represented by the nodes on the sides above and below the piezoelectric patches; the potentials on the electrodes in contact with the core of the section are fixed to zero, so that the electric fields have the same direction of the material polarization (direction 3 of Tab. 1).

The computed stiffness matrix is reported in Tab. 2. A three dimensional beam of length 2 m has been analyzed with Abaqus, with isostatic constraints applied on one of the sections. Two load conditions are considered. In the first one an electric potential of 1000 V is applied on both electrodes. In the second one the same electric potential is applied on the lower electrode only. In order to compare the deformations obtained with the present method and the

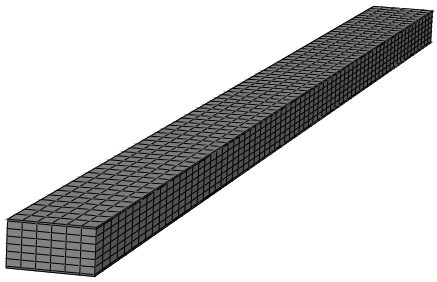

Figure 3: Rectangular section beam Abaqus model.

	both electrodes		lower electrode	
	Present	Abaqus	Present	Abaqus
Axial deformation ψ_z	-7.9159E-5	-7.8498E-5	-3.958E-5	-3.8671E-5
Curvature γ_x	0.0	0.0	2.1623E-3	2.1072E-3

Table 3: Rectangular section beam: deformation obtained by applying a 1000 V potential to both (left) and one (right) electrodes.

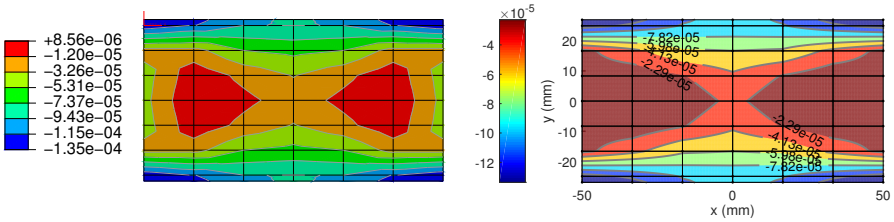

Figure 4: Triangular section beam with 100 V applied on the lower electrode: ϵ_{11}. Abaqus 3D model (left) and present beam section model (right).

ones obtained with the three dimensional model, the results of the latter needs to be post-processed. The axial beam deformation is estimated as the mean value, computed over the section, of the three dimensional axial deformation. The curvature around the y axis is estimated as the derivative of the section rotation, and is computed by dividing the rotation of the end section by the total beam length. Table 3 compares the computed deformations.

Figures 4 and 5 compare the deformation field $\epsilon_{11}$and ϵ_{12} predicted, when an electric potential of 1000 V is applied on both electrodes. They are based on the Abaqus model and the proposed section characterization procedure. It should be remarked that the contouring algorithms used by Abaqus and by the present beam section code are different. Abaqus plots the contour after computing, for each material domain, the nodal average of a deformation. The beam section code, instead, post-processes a deformation by projecting it onto the same finite element space used to approximate its parent displacement.

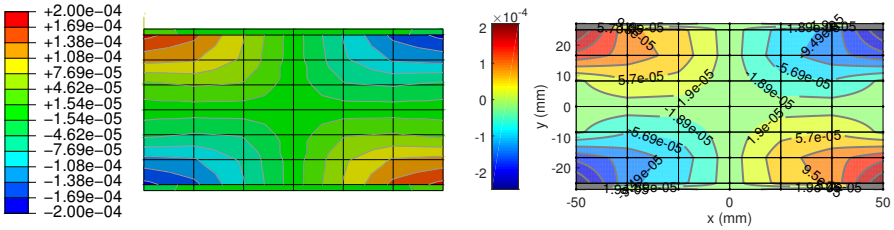

Figure 5: Triangular section beam with 100 V applied on the lower electrode: ϵ_{12}. Abaqus 3D model (left) and present beam section model (right).

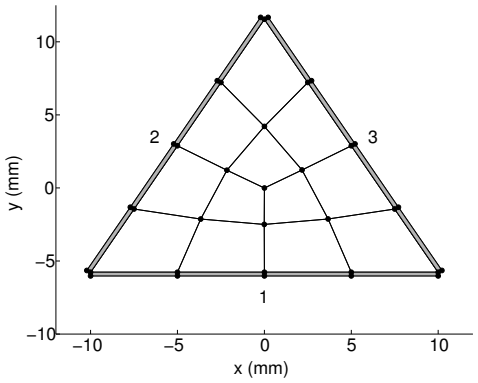

Figure 6: Triangular section.

	$\boldsymbol{K}_{\psi\psi}$	
	Present	ANBA
EA, N	1.4915E+6	1.4915E+6
$(GA)_x$, N	3.7123E+5	3.70485E+5
$(GA)_y$, N	3.7122E+5	3.70485E+5
GJ, Nm^2	1.8189E+1	1.8156E+1
$(EJ)_x$, Nm^2	4.0748E+1	4.0749E+1
$(EJ)_y$, Nm^2	4.0747E+1	4.0749E+1

	$\boldsymbol{K}_{VV}$	
	Present	ANBA
C_{ViVi}, F/m	1.9269E-6	1.9303E-6
$C_{ViVj,i\neq j}$, F/m	-1.7807E-8	-2.075E-8

	$\boldsymbol{K}_{\psi V}$	
	Present	ANBA
T_{zV1}, C/m	0.32549	0.3255
T_{zV2}, C/m	0.32549	0.3255
T_{zV3}, C/m	0.32549	0.3255
M_{xV1}, C	-1.9486E-3	-1.929E-3
M_{xV2}, C	9.741E-4	9.77E-4
M_{xV3}, C	9.741E-4	9.77E-4
M_{yV1}, C	2.3E-8	2.8E-10
M_{yV2}, C	1.685E-3	1.6927E-3
M_{yV3}, C	-1.685E-3	-1.6927E-3

Table 4: Triangular section beam properties.

5.2. Example 2 : Triangular section

The triangular section of Fig. 6 was first considered in Ghiringhelli et al. (1997). The section core is made of epoxy resin, with three piezoelectric patches attached to each side of the beam. The polarization direction of the piezoelectric materials is normal to the sides of the section and points to the host structure center. The three inner electrodes are unloaded, with the electric potential applied to the outer ones. The electrodes are numbered as in Fig. 6. The beam core sides are 0.02 m wide; the piezoelectric patches are .25 mm thick. The beam section has 4 elements on each side, with one element through the thickness for the piezoelectric patches. The center of the triangular section is located in the origin of the reference system. The results, shown in Table 4, are almost indistinguishable from those reported in Ghiringhelli et al. (1997), obtained with the ANBA code. As for the previous example, the behavior of a three dimensional beam of length 0.5 m has been analyzed with Abaqus. Two load conditions are considered. In the first one an electric potential of 100 V is

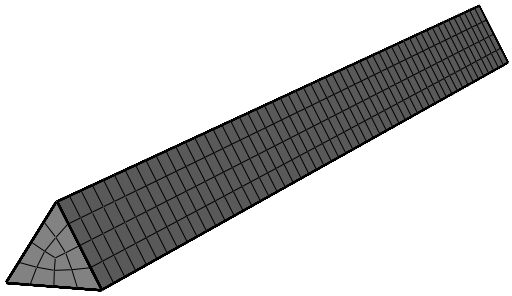

Figure 7: Triangular section beam Abaqus model.

	all electrodes		lower electrode	
	Present	Abaqus	Present	Abaqus
Axial deformation ψ_z	-6.547E-5	-6.4235E-5	-2.1823E-5	-2.1409E-5
Curvature γ_x	0.0	0.0	0.478E-2	0.466E-2

Table 5: Deformation due to a 100 V applied to all electrodes (left) and to the lower electrode (right).

applied on each electrode; only the lower electrode is loaded in the second load condition. The deformations of the three dimensional model are post-processed as in the previous example. As can be seen form Tab. 5 the results obtained with the three dimensional model and the proposed method show a good agreement. Figures 8 and 9 compare the deformation fields $\epsilon_{11}$and ϵ_{12}, as predicted, for this case, by the three dimensional Abaqus model and the proposed section characterization procedure.

This test case is used as a mean to verify the effectiveness of modeling this kind of structures as beams characterized by the computed stiffness matrix. To do so, the axis displacement due to 100 V on the left electrode is computed

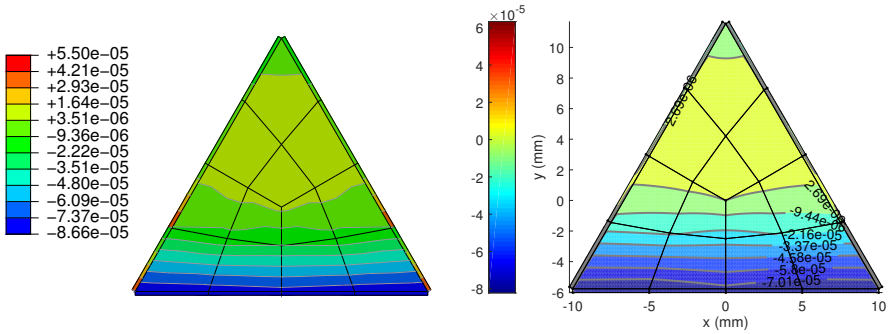

Figure 8: Triangular section beam with 100 V applied on the lower electrode: ϵ_{11}. Abaqus 3D model (left) and present beam section model (right).

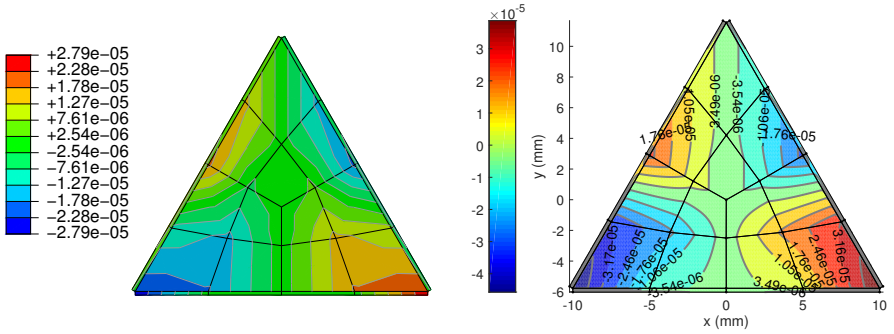

Figure 9: Triangular section beam with 100 V applied on the lower electrode: ϵ_{12}. Abaqus 3D model (left) and present beam section model (right).

	Present	Abaqus
s_x, m	-4.954E-4	-4.986E-4
s_y, m	2.860E-4	2.879E-4
s_z, m	-1.091E-5	-1.063E-5

Table 6: Displacements of the end section.

by means of a beam model and compared with that of the three dimensional FEM analysis. The beam model uses the stiffness matrix of Tab. 4 and has the same discretization along the beam axis of the three dimensional model. Table 6 compares the beam end section displacements with the average end section displacements of the 3D FEM model.

5.3. Example 3 : Two layered beam

The case study analyzed by Roy et al. (2007) is considered. The rectangular cross section is composed of an aluminum layer bounded to a thick piezoelectric layer. A voltage of 10 kV is applied on the surface of the piezoelectric material, with the interface between the piezoelectric and the aluminum layers grounded. The piezoelectric material is polarized along the global y axis, that corresponds to the piezolectric local z axis. Both layers are 5 mm thick and the section is 20 mm wide. The mesh, shown in Fig. 10, has 40x8 elements. The aluminum elastic modulus is equal to $E = 68.9$ GPa, its Poissson coefficient to $\nu = 0.25$. The properties of the piezoelectric material are reported in Tab. 7.

The computed stiffness matrix is shown in Tab. 8. The results are compared with those reported by Roy et al. (2007); however, no comparison is possible for the shear stiffness since that work is based on the variational asymptotic method. The only significant difference in Tab. 8 is that for the torsional stiffness GJ, 122.18 Nm^2 vs. 130.04 Nm^2. At a first glance, this could be imputed to the fact that VABS results are computed using 80 8-noded parabolic elements, while the present results are computed by using 320 4-noded bilinear elements. However, increasing the number of elements from 320 to 5120 brings the torsional stiffness from 122.18 Nm^2 down to 121.78 Nm^2.

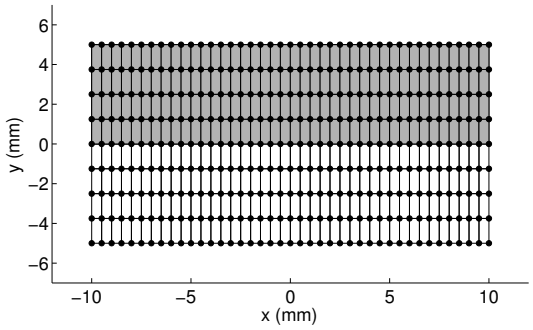

Figure 10: Two layered section.

	PZT4
$E_{11} = E_{22}$, GPa	8.13E+1
E_{33}, GPa	6.45E+1
ν_{12}	0.329
$\nu_{13} = \nu_{23}$	0.432
G_{12}, GPa	3.06E+1
$G_{13} = G_{23}$, GPa	2.56E+1
$\mathcal{E}_{311} = \mathcal{E}_{322}$, C/m^2	-5.2
$\mathcal{E}_{333}$, C/m^2	1.508E+1
$\mathcal{E}_{212} = \mathcal{E}_{123}$, C/m^2	1.27E+1
$\epsilon_{11} = \epsilon_{22}$, F/m	6.761E-9
ϵ_{33}, F/m	5.874E-9

Table 7: Material properties.

	$\boldsymbol{K}_{\psi\psi}$	
	Present	VABS
EA, N	1.5026E+7	1.5026E+7
$K_{M_x s_z}$, Nm	3.0589E+3	3.0622E+3
$K_{T_x s_y}$, Nm	1.7179E+5	—
$K_{M_z s_x}$, Nm	1.1645E+3	—
$(GA)_x$, N	4.4191E+6	—
$(GA)_y$, N	4.2307E+6	—
GJ, Nm^2	1.2218E+2	1.3004E+2
$(EJ)_x$, Nm^2	1.2796E+2	1.2777E+2
$(EJ)_y$, Nm^2	5.0096E+2	5.0081E+2

	$\boldsymbol{K}_{\psi V}$	
	Present	VABS
T_{zV}, C/m	-0.20263	-0.20245
M_{xV}, C	-4.832E-4	-4.8434E-4

	$\boldsymbol{K}_{VV}$	
	Present	VABS
C, F/m	4.0073E-8	—

Table 8: Comparison with the VABS method.

6. Conclusions

An improved general method for modeling anisotropic, straight and linear beam sections with embedded piezoelectric devices is presented. The stiffness matrix per unit length of the beam is correctly evaluated by accounting for a completely coupled three-dimensional piezoelectric constitutive law. To do so, the homogeneous solutions, i.e. the the so-called de Saint-Venant's solutions, are considered along with a set of particular solutions obtained by independently loading the beam piezoelectric patches with an electric potential. The new formulation does not requires any redundant assumption, thus allowing to straightforwardly develop the related model and compute the generalized constitutive law of a beam section. No asymptotic expansion is required, so that the obtained results keep valid independently from the beam slenderness. The proposed approach is validated through three-dimensional finite element models and similar semi-analytical methods.

The method could be easily extended to more general applications.

Appendix

This Appendix reports the expressions required to assemble the matrices of Eq. 11. They are obtained taking into account the symmetries of the elastic tensor $\mathbb{E}$, the symmetry of the third order tensor $\mathcal{E} = \mathcal{E}^{T132}$ and the symmetry of the second order tensor $\boldsymbol{\varepsilon} = \boldsymbol{\varepsilon}^T$. The domain of integration E is the area of a single finite element. All the sub-matrices have to be assembled, as it is customary to do.

$$\boldsymbol{M}_{uu}(i,j) = \int_E N_i N_j \boldsymbol{n} \cdot \mathbb{E} \cdot \boldsymbol{n} \mathrm{d}A \tag{37}$$

$$\boldsymbol{M}_{uV}(i,j) = \int_E N_i N_{pj} \boldsymbol{n} \cdot \mathcal{E}^{T231} \cdot \boldsymbol{n} \mathrm{d}A \tag{38}$$

$$\boldsymbol{M}_{VV}(i,j) = \int_E N_{pi} \boldsymbol{n} \cdot \boldsymbol{\varepsilon} \cdot \boldsymbol{n} N_{pj} \mathrm{d}A \tag{39}$$

$$\boldsymbol{C}_{uu}(i,j) = \int_E N_{i/\otimes S} \cdot \mathbb{E} \cdot \boldsymbol{n} N_j \mathrm{d}A \tag{40}$$

$$\boldsymbol{C}_{uV}(i,j) = \int_E N_i \boldsymbol{n} \cdot \mathcal{E}^{T231} \cdot N_{pj/\otimes S} \mathrm{d}A \tag{41}$$

$$\boldsymbol{C}_{Vu}(i,j) = \int_E N_{pi/\otimes S} \cdot \mathcal{E} \cdot \boldsymbol{n} N_j \mathrm{d}A \tag{42}$$

$$\boldsymbol{C}_{VV}(i,j) = \int_E N_{pi/\otimes S} \cdot \boldsymbol{\varepsilon} \cdot \boldsymbol{n} N_{pj} \mathrm{d}A \tag{43}$$

$$\boldsymbol{E}_{uu}(i,j) = \int_E N_{i/\otimes S} \cdot \mathbb{E} \cdot N_{j/\otimes S} \mathrm{d}A \tag{44}$$

$$\boldsymbol{E}_{uV}(i,j) = \int_E N_{i/\otimes S} \cdot \mathcal{E}^{T231} \cdot N_{pj/\otimes S} \mathrm{d}A \tag{45}$$

$$\boldsymbol{E}_{VV}(i,j) = \int_E N_{pi/\otimes S} \cdot \boldsymbol{\varepsilon} \cdot N_{pj/\otimes S} \mathrm{d}A \tag{46}$$

Bibliography

Aldraihem, O. J., Khdeir, A. A., 2000. Smart beams with extension and thickness-shear piezoelectric actuators. Smart Materials and Structures 9.

Bauchau, O. A., Han, S., in press. Three-dimensional beam theory for flexible multibody dynamics. Journal of Computational and Nonlinear Dynamics.

Benjeddou, A., 2000. Advances in piezoelectric finite element modeling of adaptive structural elements: a survey. Computers and Structures 76, 347–363.

Benjeddou, A., Trindade, M. A., Ohayon, R., 1997. A unified beam finite element model for extension and shear piezoelectric actuation mechanisms. Journal of Intelligent Material Systems and Structures 8, 1012–1025.

Carpenter, M. J., 1997. Using energy methods to derive beam finite elements incorporating piezoelectric materials. Journal of Intelligent Material Systems and Structures 8.

Censik, C. E. S., Ortega-Morales, M., 2001. Active beam cross-sectional modeling. Journal of Intelligent Material Systems and Structures 12.

Chakravarty, U. K., Jun. 2011. On the modeling of composite beam cross-sections. Composites Part B: Engineering 42 (4), 982–991.
URL `http://www.sciencedirect.com/science/article/pii/S1359836811000291`

Elshafei, M. A., Alraiess, F., 2013. Modeling and analysis of smart piezoelectric beams using simple higher order shear deformation theory. Smart Materials and Structures 22.

Ghiringhelli, G. L., Masarati, P., Mantegazza, P., 1997. Characterization of anisotropic non-homogeneous beam section with embedded piezo-electric materials. Journal of Intelligent Material Systems and Structures 8 (10), 842–858.

Ghiringhelli, G. L., Masarati, P., Morandini, M., Muffo, D., 2008. Integrated aeroservoelastic analysis of induced strain rotor blades. Mechanics of Advanced Materials and Structures 15, 291–306.

Giavotto, V., Borri, M., Mantegazza, P., Ghiringhelli, G. L., Carmaschi, V., Maffioli, G. C., Mussi, F., 1983. Anisotropic beam theory and applications. Computers & Structures 16, 403–413.

Hodges, D. H., 2006. Nonlinear composite beam theory. No. 213 in Progress in Astronautics and Aeronautics. American Institute of Aeronautics and Astronautics, 1801 Alexander Bell Drive, Suite 500, Reston, VA, 20191-4344, USA.

Leung, A., Zheng, J., Lim, C., Zhang, X., Xu, X.-S., Gu, Q., Oct. 2008. A new symplectic approach for piezoelectric cantilever composite plates. Computers & Structures 86 (19–20), 1865–1874.
URL http://www.sciencedirect.com/science/article/pii/S0045794908000953

Maurini, C., Pouget, J., dell'Isola, F., 2004. On a model of layered piezoelectric beams including transverse stress effect. International Journal of Solids and Structures 20.

Mielke, A., 1991. Hamiltonian and Lagrangian Flows on Center Manifolds with Applications to Elliptic Variational Problems. Vol. 1489 of Lecture Notes in Mathematics. Springer Berlin / Heidelberg.

Morandini, M., Chierichetti, M., Mantegazza, P., May 2010. Characteristic behavior of prismatic anisotropic beam via generalized eigenvectors. International Journal of Solids and Structures 47 (10), 1327–1337.

R. Zemcik, P. S., 2007. Modal analysis of beam with piezoelectric sensors a actuators. Applied and Computational Mechanics 1, 381–386.

Rao, K. S., Srinivas, G., Prasad, M. S., Srinivas, Y., Shudheer, B., Rao, A. V., 2012. Design and simulation of mems based piezoelectric shear actuated beam. American Journal of Materials Science 2, 179–184.

Roy, S., Yu, W., Han, D., 2007. An asymptotically correct classical model for smart beams. International Journal of Solids and Structures 44, 8424–8439.

Shin, S. J., Censik, C. E., 2007. Helicopter vibration reduction in forward flight using blade integral twist actuation. Journal of Mechanical Science and Technology 21 (2).

T C Manjunath, B. B., 2006. Multivariable control of smart timoshenko beam structures using pof technique. International Journal of Signal Processing.

ur Rahman, N., Alam, M. N., 2012. Active vibration control of a piezoelectric beam using pid controller: Experimental study. Latin American Journal of Solids and Structures 9, 657–673.

Wanxie, Z., Xinsheng, X., Hongwu, Z., 1996. Hamiltonian system and the saint venant problem in elasticity. Applied Mathematics and Mechanics 17 (9), 827–836.
URL http://dx.doi.org/10.1007/BF00127182

Yao, W., Zhong, W., Lim, C. W., Feb. 2009. Symplectic Elasticity. WORLD SCIENTIFIC.
URL http://www.worldscientific.com/worldscibooks/10.1142/6656